JOURNAL OF MATERIALS SCIENCE **40** (2005) 1917– 1922

Synthesis of magnetic nanocomposite $MgO/MgFe_2O_4$ from Mg-Fe layered double hydroxides precursors

FENG LI, QIAOZHEN YANG, DAVID G. EVANS, XUE DUAN*
Education Ministry Key Laboratory of Science and Technology of Controllable Chemical Reactions, P.O. Box 98, Beijing University of Chemical Technology, Beijing 100029, People's Republic of China
E-mail: duanx@mail.buct.edu.cn

The present letter reported the synthesis of MgO-containing magnetic nanocomposites by calcinations of tailored hydrotalcite-like layered double hydroxides (LDHs) of the type $[Mg_{1-x-y}Fe^{2+}_yFe^{3+}_x(OH)_2]^{x+}(A)_{x/2}\cdot mH_2O$ ($y \geq 0$; $A = CO_3^{2-}$ or SO_4^{2-}) precursors at 900°C for 2 h. The results indicate that calcination of LDHs gives rise to the formation of magnetic nanocomposites of MgO and $MgFe_2O_4$ spinel ferrite, where MgO formed could disperse and separate $MgFe_2O_4$ particles, and MgO itself was also dispersed or embedded uniformly in the $MgFe_2O_4$ spinel matrix. Furthermore, initial studies on the bactericidal properties with *staphylococcus aureus* show that these as-synthesized nanometer-sized materials have significant bactericidal effect, which increases with the increasing volume fraction of MgO.

1. Introduction

Studies of materials with nanometer-sized particles (1–100 nm in diameter) have been very progressive during past years because of the dependence of the new physicochemical properties of materials on nanoparticle size [1]. One of the interesting groups consists in metal oxide compounds, e.g., ultra fine and nanoscale magnesium oxide particles with interesting basic property and high specific surface area have many applications. In particular, they have shown great promise as destructive adsorbent for toxic chemical agents [2], and as bactericidal agents [3]. Moreover, Klabunde and coworkers have also found that magnesium oxide nanoparticles with adsorbed elemental chlorine are quite active as biocides [4]. Magnesium oxide is obtained mainly by thermal decomposition of magnesium hydroxide or carbonate [5] and by the sol–gel process [6], which are closely related to the morphology and particle size.

Layered double hydroxides (LDHs), also known as hydrotalcite-like materials, are a class of synthetic two-dimensional nanostructured anionic clays whose structure can be described as containing brucite-like layers in which a fraction of the divalent cations have been replaced isomorphously by trivalent cations giving positively-charged sheets with charge-balancing anions between the layers [7]. LDHs have the general formula $[M^{2+}_{1-x}M^{3+}_x(OH)_2]^{x+}(A^{n-})_{x/n}\cdot mH_2O$, where M^{2+} and M^{3+} are di- and trivalent cations respectively, including Mg^{2+}, Fe^{2+}, Co^{2+}, Cu^{2+}, Ni^{2+}, or Zn^{2+} and Al^{3+}, Cr^{3+}, Ga^{3+}, Mn^{3+} or Fe^{3+}, respectively; x is equal to the molar ratio of $M^{2+}/(M^{2+} + M^{3+})$; and A^{n-} is an anion, such as CO_3^{2-}, SO_4^{2-}, NO_3^-, F^-, Cl^- or PO_4^{3-} [8]. Therefore, a large class of isostructural materials considered complementary to aluminosilicate clays with widely varied physicochemical properties can be obtained by changing the nature of metal cation, the molar ratio of M^{2+}/M^{3+} as well as the type of the interlayer anion. These materials are potentially attractive precursors for spinel ferrites since they are often formed with mixtures of the same cations and have been shown to have an absence of long-range cation ordering [9]. Calcination of LDHs at intermediate temperatures (450–600°C) affords poorly crystalline mixed metal oxides [10]. Calcination above 750°C is known to give spinel ferrites, but these are always mixed with the oxide of divalent metal [11]. This reflects the fact that in LDHs, the divalent cations are always present in greater amount than the trivalent cations (the stoichiometric x above is found typically in the range 0.2–0.33, corresponding to the molar ratio of M^{2+}/M^{3+} of 2–4). However, we have synthesized successfully pure magnetic $MgFe_2O_4$ spinel ferrite with nanoscale crystallite size and high saturation magnetization by calcination of tailored Mg-Fe^{2+}-Fe^{3+}-LDHs containing interlayer carbonate or sulphate ions [12, 13], because oxidation of Fe^{2+} ions on the lattice of LDHs at high calcination temperatures in air can give additional Fe^{3+} ions, and thus overcoming the deficiency of trivalent ions.

*Author to whom all correspondence should be addressed.

On the basis of the above facts, it is rather possible that nanocomposites containing a small amount of MgO dispersed or embedded in a large amount of $MgFe_2O_4$ spinel matrix can be prepared by calcinations of tailored hydrotalcite-like layered double hydroxides (LDHs) containing Mg^{2+}, Fe^{3+} and/or Fe^{2+} cations on the lattices. Furthermore, these as-synthesized materials may be suitable as bactericidal agents due to the presence of nanoscale magnesium oxide formed. In addition, as magnetic materials they combine the advantages of being easy to separate and recover at magnetic field, and not inclining to causing loss and pollution because they do not retain any magnetism after removing the magnetic field. Therefore, in this paper, we focus attention on the synthesis of LDHs of the type $[Mg_{1-x-y}Fe_y^{2+}Fe_x^{3+}(OH)_2]^{x+}(A)_{x/2}\cdot mH_2O$ ($y \geq 0$; $A = CO_3^{2-}$ or SO_4^{2-}) precursors. The purpose is to characterize the phase compositions of the resulting calcined LDHs by dependence on the Mg/Fe molar ratio. And initial studies on the bactericidal properties of these calcined materials have also been carried out.

2. Experimental

2.1. Preparation of samples

Layered double hydroxides sulphate containing Mg^{2+}, Fe^{2+} and Fe^{3+} ions (Mg-Fe^{2+}-Fe^{3+}-SO_4-LDHs) were prepared by coprecipitation method under nitrogen atmosphere (in order to minimize the contamination with atmospheric CO_2). A mixed salt solution of $Fe_2(SO_4)_3$, $FeSO_4$ and $MgSO_4$ was dissolved in N_2-saturated deionized water ($[Mg^{2+} + Fe^{2+} + Fe^{3+}] = 1.2$ mol/L). A base solution ([NaOH] = 1.5 M) in N_2-saturated deionized water was added dropwise to the stirred the mixed salt solution at 25°C until the pH reached 10.0. The resulting suspension was aged at 40°C for 4 h under N_2 atmosphere. The mixture was cooled, filtered and washed with N_2-saturated deionized water at 0°C, and then N_2-saturated ethanol at 0°C. The final gelatinous precipitate was dried at room temperature and stored at 0°C under N_2. Layered double hydroxides carbonate containing Mg^{2+} and Fe^{3+} ions (Mg-Fe^{3+}-CO_3−LDHs) were prepared by coprecipitation method. A base solution of NaOH and Na_2CO_3 ($[CO_3^{2-}] = 2[Fe^{3+}]$, $[OH^-] = 2\{2[Mg^{2+}] + 3[Fe^{3+}]\}$) was added dropwise with vigorous stirring to an aqueous mixed salt solution containing $Mg(NO_3)_2$ and $Fe(NO)_3$ ($[Mg^{2+} + Fe^{3+}] = 1.2$ mol/L) at 25°C until the pH reached 10.0. The resulting suspension was aged with stirring at 100°C for 4 h. The mixture was cooled, filtered and washed with deionized water. The resulting solid was dried at 60°C for 24 h. The above-synthesized LDHs precursors were calcined at 900°C for 2 h in air, and then the resulting products were slowly cooled to room temperature.

2.2. Characterization

Powder X-ray diffraction (XRD) patterns of the samples were recorded using a Rigaku XRD-6000 diffractometer under the following conditions: 40 kV, 30 mA, graphite-filtered Cu-Kα radiation ($\lambda = 0.15418$ nm). The samples, as unoriented powders, were step-scanned in steps of 0.04° (2θ) using a count time of 10 s/step.

Elemental analysis was performed using a Shimadzu ICPS-75000 inductively coupled plasma emission spectrometer (ICP-ES) for metal ions. Samples were dried at 100°C for 24 h prior to analysis, and solutions were prepared by dissolving the samples in dilute hydrochloric acid (1:1).

Fourier transform infrared (FT-IR) spectra were recorded in the range 4000 to 400 cm^{-1} with 2 cm^{-1} resolution on a Bruker Vector-22 Fourier transform spectrometer using the KBr pellet technique (1mg of sample in 100 mg of KBr).

The specific area was determined from N_2 adsorption measurements in a Sorptomatic1990 automatic gas adsorption instrument. Prior to the measurements, samples were degassed at 200°C under vacuum for 2 h. Specific surface area was calculated from according to the Brunauer–Emmett–Teller (BET) method.

Transmission Electron Microscopy (TEM) studies were performed using a Hitachi H-800 model machine for high-resolution observation. The accelerating voltage applied was 100 kV.

Mössbauer spectra were recorded with an Oxford MS-500 instrument at 293 K. A radiation source of Co^{57} in an Rh matrix was used. The isomer shifts are reported relative to sodium nitroprusside.

The magnetic measurement of samples was taken on a locally made JDM-13 vibration sample magnetometer (VSM) in an applied magnetic field of 15 KOe. Metal nickel powder as a standard sample calibrated for error in the test.

2.3. Sterilization test with staphylococcus aureus

Aqueous suspension of 1.0 wt% for the calcined LDHs in a tube was put into a boiling pot under high pressure for 1 h, then fresh cultivated *staphylococcus aureus* suspension was dropped into the tube, where *staphylococcus aureus* had a concentration 10^5CFU (colony forming units)/mL. After the calcined LDHs reacted with *staphylococcus aureus* at 37°C for 2 h, the reaction system was diluted with water and the test was kept for 24 h.

3. Results and discussion

3.1. Structure of the LDHs

Fig. 1 illustrates the powder XRD patterns for Mg-Fe^{2+}-Fe^{3+}-SO_4-LDHs and Mg-Fe^{3+}-CO_3-LDHs with the different Mg/Fe molar ratios in the synthesis mixture, whilst Table I summarizes the analytical and structural data of LDHs. Obviously, note that in each case the XRD patterns exhibit the characteristic diffractions of hydrotalcite-like layered double hydroxide materials [11, 14] and no other crystalline phases are present. The most close XRD patterns for LDHs containing interlayer sulfate (see Fig. 1a and b) and LDHs containing interlayer carbonate (see Fig. 1c and d) are JCPDS file No. 39-0338 and JCPDS file No. 38–0487, respectively. Moreover, the XRD patterns exhibit the

TABLE I Structure and component of the synthesized LDHs

Sample	LDH-a	LDH-b	LDH-c	LDH-d
Initial $Mg^{2+}/Fe^{2+}/Fe^{3+}$ molar ratio	4:5:2	5:5:2	2:0:1	3:0:1
Initial $(Mg^{2+} + Fe^{2+})/Fe^{3+}$ molar ratio	4.5	5.0	2.0	3.0
Initial Mg/Fe molar ratio	0.571	0.714	2.0	3.0
Lattice parameter a (nm)	0.314	0.315	0.310	0.310
Lattice parameter c (nm)	3.253	3.262	2.301	2.324
Final Mg/Fe molar ratio in LDHs	0.534	0.723	2.190	3.191

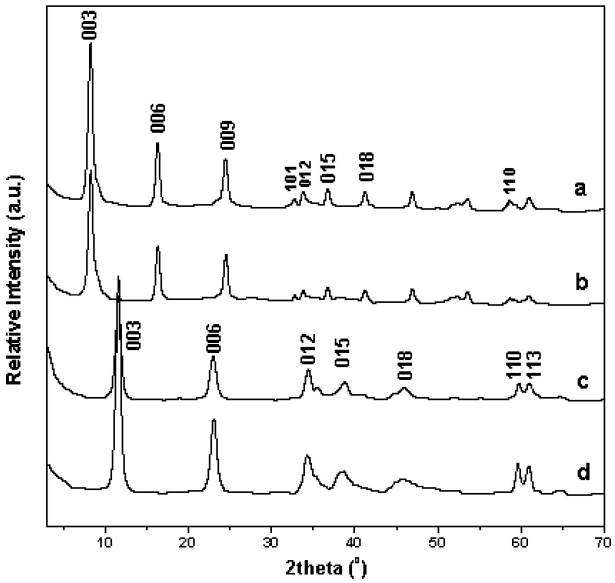

Figure 1 Powder XRD patterns of Mg-Fe-LDHs: (a) LDH-a, (b) LDH-b, (c) LDH-c, and (d) LDH-d.

sharp characteristic diffraction lines appearing as symmetric lines at low 2θ angle, corresponding to the basal spacing and its higher order diffractions, as indicates that the samples consist of a well crystallized single phase. Compared to the XRD patterns for Mg-Fe^{3+}-CO_3-LDHs, those for Mg-Fe^{2+}-Fe^{3+}-SO_4-LDHs show out a smaller degree displacement of (003) diffraction line denoting an increase in the basal spacing (d_{003}) due to the presence of different interlayer anions, sulfate and carbonate ions. Meanwhile, it can be seen from Table I that the final Mg/Fe molar ratios in the products are close to those in the synthesis mixture. It suggests that almost all the metal ions can be coprecipitated completely.

It is well known that LDH is a hexagonal system, where the lattice parameter a is a function of the average radii of metal ions within the layers and reflects the density of metal ions stacking in 003 crystal plane, whilst the lattice parameter c is three times the distance from the center of one layer to the next and is a function of the average charge of the metal ions, the nature of the interlayer anion and the interlayer water content. Assuming a 3R stacking of the layers and from the positions of the (003) and (110) diffractions, although the latter (the lower angle component of the characteristic doublet diffractions close to $2\theta = 59^\circ$) is rather broad and ill-defined, the lattice parameters a and c dependent

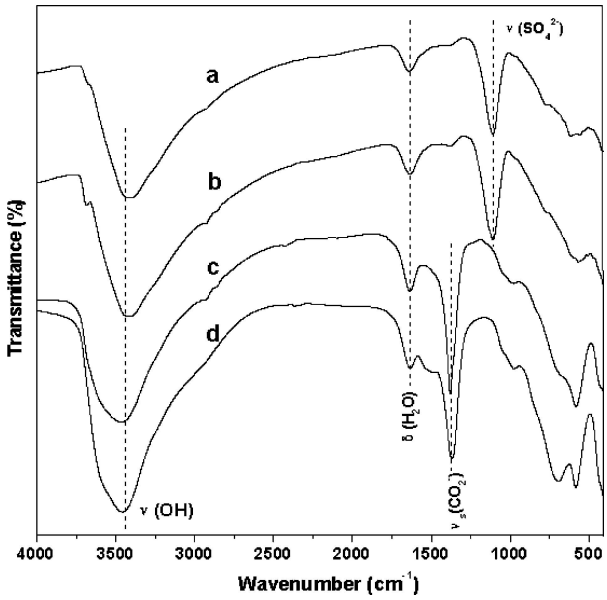

Figure 2 FT-IR spectra for LDHs: (a) LDH-a, (b) LDH-b, (c) LDH-c, and (d) LDH-d.

of the composition of LDHs may be calculated [15]. As shown in Table I, with increasing the content of Fe^{2+} ions, the lattice parameter a ($= 2d_{110}$) increases gradually, reflecting the fact that the Shannon ionic radii for octahedral high spin Fe^{2+}, Mg^{2+} and Fe^{3+} are 0.092, 0.086 and 0.079 nm, respectively. The lattice parameter c ($= 3d_{003}$) has been shown to increase with increasing M^{2+}/M^{3+} molar ratio when the interlayer anion is identical. This is consistent with the decrease in Coulombic attractive force between the negatively charged interlayer anions and the positively charged brucite-like layers as the proportion of trivalent ions in the latter decreases. Furthermore, as expected, the values of the lattice parameter c for the Mg-Fe^{2+}-Fe^{3+}-SO_4-LDHs are much bigger than those for Mg-Fe^{3+}-CO_3-LDHs due to different interlayer anions.

The FT-IR spectra of the as-synthesized LDHs in the region between 400 and 4000 cm^{-1} are illustrated in Fig. 2. In general the strong and broad band observed around 3600–3200 cm^{-1} corresponds to the O–H stretching vibration of surface and interlayer water molecules [7], which are found at lower frequency in LDHs compared with the O–H stretching vibration in free water at 3600 cm^{-1} [16]. This is related to the formation of hydrogen bonding of interlayer water with the guest anions as well as with hydroxide groups of layers [17]. The adsorption at 1635 cm^{-1} is assigned to the bending vibration of water, $\delta(H_2O)$. The FT-IR spectra of Mg-Fe^{3+}-CO_3-LDHs show an intense band at around 1382 cm^{-1} associated with the symmetric stretching mode of interlayer carbonate anion, whilst there is an absorption at around 1107 cm^{-1}, which arises from the symmetric stretching mode of the interlayer sulfate anion of Mg-Fe^{2+}-Fe^{3+}-SO_4-LDHs. The bands observed in the low-frequency region of the spectrum are interpreted as the lattice vibration modes and can be attributed to M-O from 850 to 600 cm^{-1} and O-M-O near 440 cm^{-1} vibrations [18].

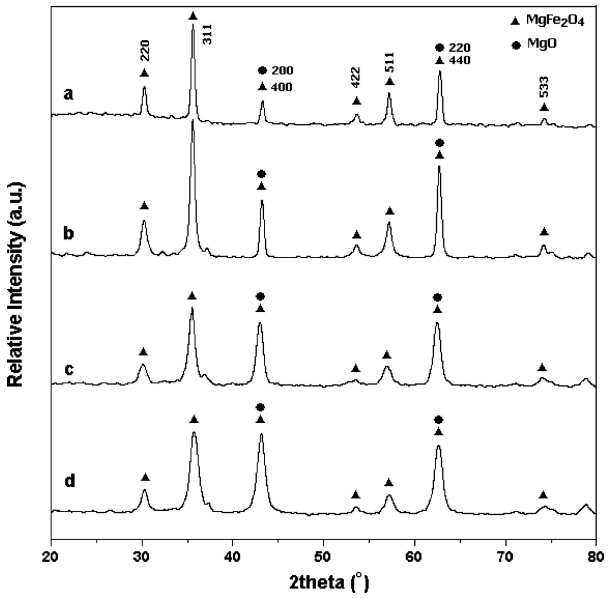

Figure 3 Powder XRD patterns for the calcined LDHs: (a) calcined LDH-a, (b) calcined LDH-b, (c) calcined LDH-c, and (d) calcined LDH-d.

3.2. Structure of the calcined LDHs

Fig. 3 displays the powder XRD patterns for the materials obtained by calcination of LDHs at 900°C for 2 h. Note that calcination has destroyed the layered structure of LDHs since no characteristic diffractions of LDHs are present. In each case the XRD spectrum exhibits a series of diffraction lines corresponding to the characteristic interplanar spacings (220), (311), (400), (422), (511) and (440) of the spinel structure. Although all of the main diffractions of MgO coincide with those of $MgFe_2O_4$, the relatively high intensities of the diffraction lines around 2θ values of 43° and 63° in the XRD pattern of calcined LDHs suggest that these are superpositions of diffractions due to the spinel phase and magnesium oxide (see Fig. 3), consistent with the high $Mg^{2+}/(Fe^{2+} + Fe^{3+})$ molar ratio in the LDHs precursors. Moreover, it can be noted that the relative intensities of (311) diffraction for $MgFe_2O_4$ to the diffraction lines around 2θ angels of 43° and 63°, respectively, are reinforced with the increasing $Mg^{2+}/(Fe^{2+} + Fe^{3+})$ molar ratio, as suggests that the volume fraction of MgO in the calcined LDHs also increased gradually, consistent with the theoretical values calculated given that LDHs are calcined completely into $MgFe_2O_4$ and MgO without other reaction phases. Mössbauer spectroscopy studies have also confirmed that there are partial overlaps of two fitted six-line subpatterns due to the small difference between the hyperfine fields of the iron atoms in the two sublattices for A-ions in tetrahedral sites and B-ions in octahedral sites, and no signals due to the existence of other phases such as Fe_2O_3 are observed, confirming that, as expected, the Fe cations of $MgFe_2O_4$ phase in all samples have a +3 oxidation state.

The average size of $MgFe_2O_4$ crystals may be estimated with the X-ray broadening analysis using the (311) diffraction line for $MgFe_2O_4$ phase by means of the well-known Scherrer equation [$L = 0.89\lambda/\beta(2\theta)cos\theta$] [19], where L is the crystallite size, λ is the wavelength of the radiation (0.15418 nm) of the radiation used, θ is the angle between the incident and diffracted beams in degrees, and $\beta(2\theta)$ is the width of the XRD pattern line at half peak height in radians. It can be seen from Table II that the all crystallite particles of $MgFe_2O_4$ lie in the nanoscale range from 36.1 to 13.5 nm, which decreases as the volume fraction of MgO increases.

Fig. 4 shows the morphological characteristics of all of the calcined samples investigated by TEM. The TEM image for the calcined LDH-a sample with the lowest amount of MgO phase clearly demonstrates the presence of regular intergranular plate-like particle, and the sizes of particles become in the range of about 100–300 nm. Furthermore, with the increasing volume fraction of MgO, the size of intergranular particle decreases gradually up to 25–55 nm in the calcined LDH-c sample. Meanwhile, it can be found that the calcined LDH-a and calcined LDH-b seem to have shown hard aggregates of sintered crystals (see Fig. 4a–b). However, the calcined LDH-d sample with the largest amount of MgO shows more apparent soft aggregates of nanoparticles, and the spherical secondary aggregated particles are composed of the no more than 20 nm primary nanoparticles. In addition, it is also evident that the data of specific surface area in all of the calcined LDHs (see Table II), which increases with the increasing volume fraction of MgO, are closely related to the sizes of composite particles by TEM, also further confirming that both of the calcined LDH-a and calcined LDH-b were present as hard aggregates of sintered $MgFe_2O_4$ crystals due to the smaller amount of MgO. The above result shows that an appropriate amount of MgO can prevents effectively migration and coalescence of $MgFe_2O_4$ particles, and thus leading to the formation of MgO/$MgFe_2O_4$ nanocomposites.

Therefore, use of a single precursor with cations distributed uniformly with no long order facilitates the synthesis of metal oxide/spinelferrite nanoparticles. The

TABLE II Structure, component and properties of the caicined LDHs

Sample	Calcined LDH-a	Calcined LDH-b	Calcined LDH-c	Calcined LDH-d
MgO (wt%) in calcined LDHs[a]	1.4	8.3	40.5	52.0
Particle size of $MgFe_2O_4$[b] (nm)	36.1	22.2	20.1	13.5
Saturation magnetization (emu/g)	22.7	21.5	14.3	11.5
Specific area (m^2/g)	1.1	2.9	58.7	65.6
Number of residual bacteria after 24 h (CFU/ml)	Too many to count	14750	10900	4700
Percent of bacteria sterilized after 24 h (%)	–	99.87	99.91	99.96

[a]Calculated theoretically (see text).
[b]Average crystallite size of $MgFe_2O_4$ obtained with Scherrer equatioin by using the (311) reflection.

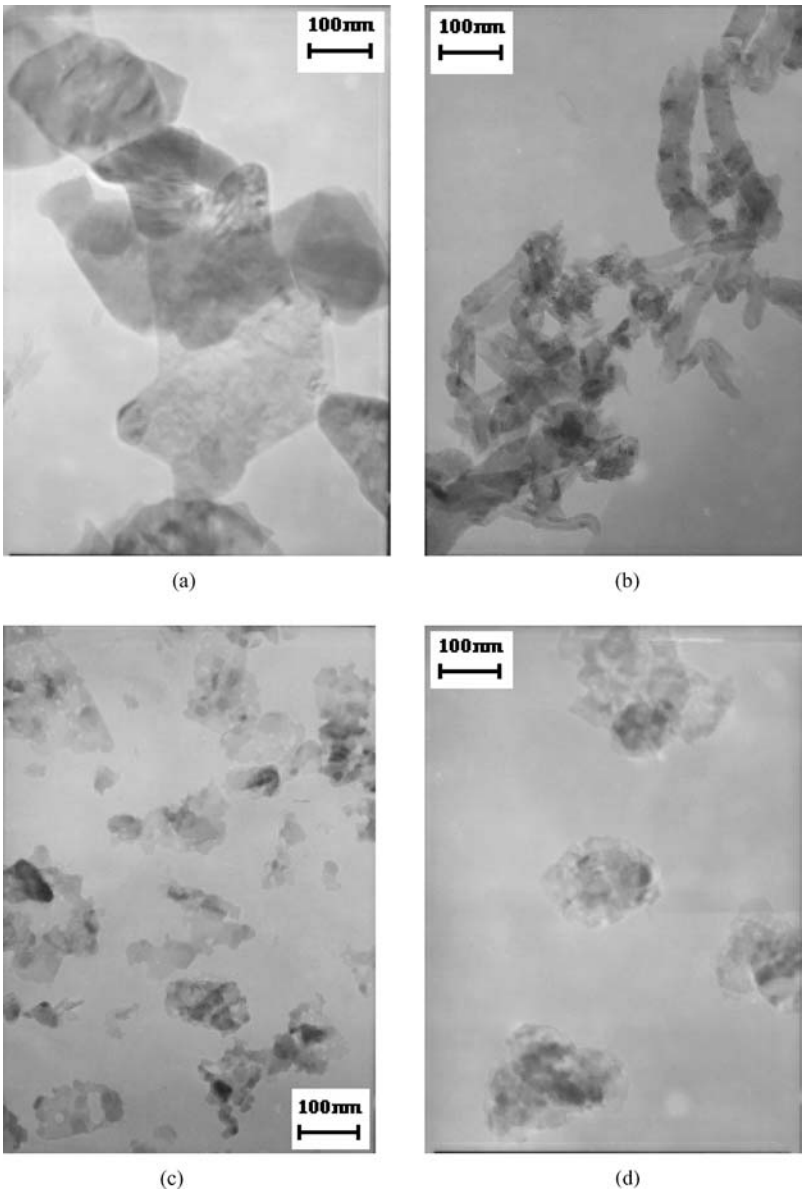

Figure 4 TEM images for the calcined LDHs: (a) calcined LDH-a, (b) calcined LDH-b, (c) calcined LDH-c, and (d) calcined LDH-d.

close structural relationship between the LDHs precursors and its calcinations products is a key factor. Rebours *et al*. have shown that collapse of the layered structure on heating an LDH at around 400°C gives a poorly crystalline mixed metal oxide which can best be described as spinel-like phase [20]. This phase preserves the particle morphology of the LDH [21], suggesting a topotactic transformation. In this case the (110) diffraction of the LDH can transform to the (440) spinel diffraction or the (220) MgO diffraction. As a result, it is clearly understood that after calcination MgOformed could disperse and separate the $MgFe_2O_4$ particles. On the contrary, MgO itself was also dispersed or embedded uniformly in the $MgFe_2O_4$ matrix.

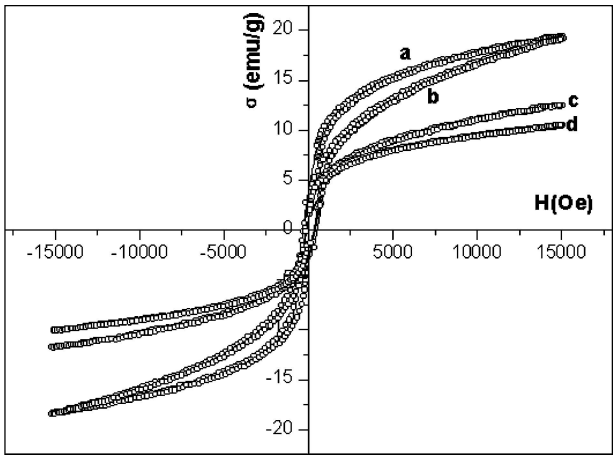

Figure 5 Hysteresis loops for the calcined LDHs: (a) calcined LDH-a, (b) calcined LDH-b, (c) calcined LDH-c, and (d) calcined LDH-d.

3.3. Magnetic and bactericidal properties of the calcined LDHs

The field dependence of the magnetization of calcined LDHs was measured at room temperature. The magnetic hysteresis loops of the samples are shown in Fig. 5. The values of the saturation magnetization evaluated by extrapolation of the M vs 1/H to 1/H = 0 are on the same order of magnitude are shown in Table II. As expected, the saturation magnetization increases from 11.5 to 22.7 emu/g with increasing

volume fraction of $MgFe_2O_4$ phase in the nanocomposites. In addition, considering the different loading weight of MgO in $MgFe_2O_4$ matrix, the saturation magnetization calculated at the same external field for single phase $MgFe_2O_4$ is 23.0, 23.4, 24.0 and 24.0 emu/g for nanocomposites with the increasing volume fraction of MgO, respectively, which are much smaller than that of pure $MgFe_2O_4$ (35.0 emu/g) reported in our previous research [13], as may possibly be attributed to the smaller nanoparticle sizes of as-produced $MgFe_2O_4$ in the kind of $MgO/MgFe_2O_4$ nanocomposites due to the dispersion effect of formed MgO on the $MgFe_2O_4$ crystallites mentioned above.

The bactericidal properties of calcined LDHs were investigated with a sterilizing *staphylococcus aureus* test. It can be seen from Table II that the calcined LDH-a with the lowest Mg/Fe molar ratio has almost not bactericidal property. However, other three magnetic nanocomposites have a significant sterilization property, which increases gradually with increasing MgO content. This is because MgO dispersed in the magnetic matrix has alkaline effect to absorb liquids inside the bacteria cells and decomposition effect [22–24] which to yield active oxygen species, such as superoxide anion radical, through enhanced structure defect by introducing transition metal element Fe species. Therefore, active oxygen species could react with organic compounds in the bacteria and decompose them into CO_2 and H_2O. On the other hand, the high efficacy of sterilization may also result from the fact that the nanoparticles can enhance surface reactivity of materials, and thus cover the bacteria cells to a high extent, as reinforces abrasion effect on the wall of the bacteria cells.

4. Conclusion

MgO-containing magnetic nanocomposites have been successfully prepared by calcinations of hydrotalcite-like layered double hydroxides (LDHs) of the type $[Mg_{1-x-y}Fe^{2+}_yFe^{3+}_x(OH)_2]^{x+}(A)_{x/2}\cdot mH_2O$ ($y \geq 0$; A = CO_3^{2-} or SO_4^{2-}) precursors at 900°C for 2 h. In these materials, the intergranular dispersed MgO particles inhibited the growth of $MgFe_2O_4$ grains, as contributed to decreasing particle size of the type of nanocomposites. The specific surface area increased with increasing volume fraction of MgO. The increased saturation magnetization was confirmed for composites containing larger amount of $MgFe_2O_4$. Initial studies on the bactericidal properties with *staphylococcus aureus* show that these $MgO/MgFe_2O_4$ nanocomposites have significant sterilizing effect, which increases with increasing molar ratio of Mg/Fe, and are potential for magnetic disinfectants. The results suggest that the method used in this study is found to be of great advantage to prepare metal oxide-containing magnetic nanocompositespossessing desirable microstructure for the multi functional composites.

Acknowledgement

We gratefully acknowledge the financial support from the National Natural Science Foundation of China (No. 90306012 and No. 20371006) and the Beijing Nova Program (No. 2003B10).

References

1. W. F. SMITH, "Principle of Materials Science Engineering" (McGraw Hill Book Company, Singapore, 1986).
2. J. V. STARK and K. J. KLABUNDE, *Chem. Mater.* **8** (1996) 1913.
3. J. SAWAI, H. KOJIMA, N. ISHIZU, M. ITOH, H. IGARASHI, T. SAWAKI and M. SHIMIZU, *J. Inorg. Biochem.* **67** (1997) 443.
4. P. K. STOIMENOV, R. L. KLINGER, G. L. MARCHIN and K. J. KLABUNDE, *Langmuir* **18** (2002) 6679.
5. B. XU, J. WEI, H. WANG, K. SUN and Q. ZHU, *Catal. Today* **68** (2001) 217.
6. H. S. CHOI and S. T. HWANG, *J. Mater. Res.* **15** (2000) 842.
7. F. CAVANI, F. TRIFIRÒ and A. VACCAN, *Catal. Today* **11** (1991) 173.
8. V. RIVES (Ed.), "Layered Double Hydroxides: Present and Future," (Nova Science Publishers, New York, 2001).
9. M. VUCELIC, W. JONES and G. D. MOGGRIDGE, *Clays Clay Miner.* **45** (1997) 803.
10. A. VACCARI, *Catal. Today* **41** (1998) 53.
11. J. M. FERNÁNDEZ, M. A. ULIBARRI, F. M. LABAJOS and V. RIVES, *J. Mater. Chem.* **8** (1998) 2507.
12. J. LIU, F. LI, D. G. EVANS and X. DUAN, *Chem. Comm.* **4** (2003) 542.
13. F. LI, J. LIU, D. G. EVANS and X. DUAN, *Chem. Mater.* **16** (2004) 1597.
14. C. BUSETTO, G. DEL PIERO, G. MAMARA, F. TRIFIRÒ and A. VACCARI, *J. Catal.* **85** (1984) 260.
15. F. MILLANGE, R. I. WALTON and D. O'HARE, *J. Mater. Chem.* **10** (2000) 1713.
16. K. NAKAMOTO, "Infrared and Raman Spectra of Inorganic and Coordination Compounds" (Wiley, New York, 1986).
17. J. T. KLOPROGGE and R. L. FROST, *J. Solid State Chem.* **146** (1999) 506.
18. M. K. TITULAER, J. B. H. JANSEN and J. W. GEUS, *Clays Clay Miner.* **42** (1994) 249.
19. W. B. INNES, in "Experimental Methods in Catalytic Research," edited by R. B. Anderson (Academic Press, New York, 1968) p. 44.
20. M. BELLOTTO, B. REBOURS, O. CLAUSE, J. LYNCH, D. BAZIN and E. ELKAIM, *J. Phys. Chem.* **100** (1996) 8535.
21. W. T. REICHLE, S. Y. KANG and D. S. EVERHARDT, *J. Catal.* **101** (1986) 352.
22. T. ASADA, M. OMICHI, T. KIMURA and K. OIKAWAA, *J. Health Sci.* **47** (2001) 414.
23. J. SAWAI, H. SHIGA and H. KOJIMA, *Intern. Biodet. Biodeg.* **47** (2001) 23.
24. C. C. TRAPALIS, P. KEIVANIDIS, G. KORDAS, M. ZAHARESCU, M. CRISAN, A. SZATVANYI and M. GARTNER, *Thin Solid Films* **433** (2003) 186.

Received 3 October 2004
and accepted 4 January 2005